

Summertime tidal flushing of Barataria Bay: Transports of water and suspended sediments

Chunyan Li,^{1,2} John R. White,¹ Changsheng Chen,^{2,3} Huichan Lin,³ Eddie Weeks,¹ Kari Galvan,¹ and Sibel Bargu¹

Received 4 August 2010; revised 19 December 2010; accepted 10 January 2011; published 13 April 2011.

[1] Inlets provide a critical ecological link between restricted bays and estuaries to the coastal ocean. The net fluxes of water and suspended sediment are presented in this study. These fluxes are obtained based on data from a multidisciplinary, full tidal cycle survey across Barataria Pass in southern Louisiana on 31 July to 1 August 2008. The velocity profiles were obtained with an acoustic Doppler current profiler mounted on a small boat continuously crossing the inlet, which contains swift and turbulent tidal currents. Water samples were collected six times in a 24 h period at three discrete depths and three locations across the inlet. The observations delineated a clear eddy on the western side of the inlet which causes a low R^2 value of the tidal harmonic analysis on the edges of the inlet. The net flux of total suspended sediment out of the bay was determined to be 8800 t of which 20% was organic matter, demonstrating a significant source of organic matter to the base of the coastal ocean detrital food chain. The time evolution and net fluxes of water, and suspended sediments showed that the net flow resembles conventional estuarine circulation patterns with net outward flow on the surface and shallow ends of the inlet and with net inward flow in the center and at the bottom of the center of the inlet. The west side has a much larger outward flow than the east side while the east side is fresher. These differences suggest that the Louisiana Coastal Current from around the Bird's Foot Delta derived from the mixing of shelf water with the Mississippi River freshwater may have entered the bay. This must have been mostly from the east side during the survey, which resulted in a smaller outward flow on the eastern side. A numerical experiment further confirmed this assumption and the model was verified by field observations on 5 May 2010.

Citation: Li, C., J. R. White, C. Chen, H. Lin, E. Weeks, K. Galvan, and S. Bargu (2011), Summertime tidal flushing of Barataria Bay: Transports of water and suspended sediments, *J. Geophys. Res.*, 116, C04009, doi:10.1029/2010JC006566.

1. Introduction

[2] The flushing of an estuary or bay is caused by river discharge, tidal oscillation and wind. The flushing process normally results in the net transport of freshwater, sediment, and land-derived carbon into the coastal ocean. The quantification of the flushing process and the calculation of the transport of waterborne materials in bays and estuaries require the knowledge of both water velocity and concentration of the substance of interest. Although computer models can provide predictions of transports, they are usually limited by a lack of information about the sources and

land side boundary conditions, which can be obtained by observations. Therefore, high-resolution measurements can be crucial in resolving transport. High-resolution measurements provide useful information for models for the purpose of verification and establishing boundary conditions. As most estuarine motions are dominated or at least influenced by tidal oscillations, such measurements must cover at least one tidal cycle or longer to resolve the tidal variations and determine net transport.

[3] In early studies, measurements of transport were accomplished by using single point current meters and discrete water sample analyses [e.g., *Kjerfve*, 1978; *Kjerfve et al.*, 1981]. With the use of acoustic Doppler current profilers (ADCP), the measurements of water velocity can be automated at high sampling frequency (~ 1 Hz) over the entire profile (a series of measurement points in the vertical or horizontal). An ADCP is a remote sensing device that measures velocity based on the Doppler frequency shifts of acoustic signals sent out by its 3–5 transducers [*RD Instruments*, 1996]. As a result, a bottom mounted or ship-mounted ADCP can often measure velocity profiles throughout the majority of the water column if

¹Department of Oceanography and Coastal Sciences, Louisiana State University, Baton Rouge, Louisiana, USA.

²College of Marine Sciences, Shanghai Ocean University, Shanghai, China.

³Department of Fisheries Oceanography, Intercampus Graduate School for Marine Science and Technology, University of Massachusetts, New Bedford, Massachusetts, USA.

the water depth is within the range of the measurements (dependent on the working frequency of the ADCP). The measurements of concentrations however are usually not through remote sensing devices and water samples have to be collected in situ. This presents a challenge when the water samples at different depths need to be collected and analyzed at various tidal phases in a swift and turbulent tidal current environment. Tides at Louisiana coast are mainly diurnal with a period of about one day [Kantha, 2005]. Therefore, to resolve the net flux, measurements have to be carried out to cover at least 24 h.

[4] More than 60 years ago, *Marmor* [1948] measured tidal currents in the passes of the Barataria Bay over a 24 day period. The amount of water going through Barataria Pass, Quatre Bayou Pass, Caminada Pass, and Pass Abel was estimated to be about 66%, 18%, 13%, and 3%, respectively, of the total. The net rate of transport was calculated to be $280 \text{ m}^3 \text{ s}^{-1}$ out of the bay system. In a more recent study, *Swenson and Swarzenski* [1995] estimated a $200 \text{ m}^3/\text{s}$ freshwater input to the Barataria system. *Snedden* [2006] used a 101 day record (20 December 2002 through 3 April 2003) from an upward looking ADCP deployed in Barataria Pass and concluded that 85% of the flow variability in the pass was tidally induced with equal contributions of the O_1 and K_1 constituents. Using an Empirical Orthogonal Function (EOF) analysis, *Snedden* [2006] showed that a barotropic mode explained $\sim 90\%$ of the total variance and a vertically sheared flow (outflows at surface opposed by inflows at the bottom), or the baroclinic mode, explained $\sim 8\%$ of the total variance. The baroclinic mode exhibited a strong coupling with diurnal tidal current amplitudes at the fortnightly time scales, with the greatest velocity shear occurring during neap tides when the tidal current amplitude is at its minimum. This indicates that the flow has a significant baroclinic component [*Nunes and Lennon*, 1987; *Nunes Vaz et al.*, 1989; *Linden and Simpson*, 1988; *Li et al.*, 1998]. In a study by *Inoue and Wiseman* [2000], a numerical model was applied to the Terrebonne and Timbalier Basin, west of the Barataria Bay. The tidal currents were demonstrated to be important, in addition to wind driven flows and a flushing time of 27 days was estimated from that study. *Inoue et al.* [2008] applied a two-dimensional model with salinity effect included for the Barataria Bay system and found that it took about 15 days for the freshwater diverted from the Mississippi River at Davis Pond Diversion facility to reach the mouth.

[5] Despite the extended studies, an accurate quantification of the tidal variations and net fluxes of water and suspended sediments have seldom been undertaken. This is especially true in the Louisiana coastal area where many important issues related to fisheries, wetland loss and water quality require more detailed understanding of the transport process through tidal passes. One of the most important issues is the fate of the nutrient flux from the Mississippi River derived from the large area of upstream agricultural activities and the impact to the coastal hypoxia [e.g., *Rabalais and Turner*, 2001; *Rabalais et al.*, 2007a, 2007b; *Justic et al.*, 2007]. The interest to this issue has prompted several modeling studies on the inner shelf [*Wang and Justic*, 2009] and in the estuaries [*Inoue and Wiseman*, 2000; *Inoue et al.*, 2008; *Park*, 2002] and it is critical to develop a better understanding on the connection between these two areas.

[6] The objective of this study is to quantify the tidal flushing process and tide-induced transport of water and suspended sediments by observations through a complete tidal cycle at a major tidal inlet connecting the Barataria Bay and the Louisiana continental shelf. Barataria Bay is adjacent to the largest river of the North America [*Benke and Cushing*, 2005], the Mississippi River. It is north of the world's second largest hypoxia region and a place with the largest wetland and disproportional rate of wetland loss (implication of sedimentation-erosion imbalance). It is one of the only two bays separating two deltas with contrasting characteristics: the Mississippi River Delta, which is experiencing severe land loss, and the Wax Lake Delta at the Atchafalaya Bay area, which is growing with greater sedimentation than erosion [*Roberts et al.*, 1980, 1997]. This area is more complicated than a classical estuary because the Mississippi River Delta provides a significant amount of freshwater discharge onto the shelf region. The main outlet of the freshwater at the Bird's Foot Delta is the Southwest Pass (Figure 1), which is about 65 km from the Barataria Pass. This is one of the major outlets of the river and it carries about 67% of the total discharge of the Mississippi River, according to our own high-resolution measurements made on 5 May 2010. Our study at Barataria Pass is based on 24 h continuous observations of hydrodynamics and water sampling, complimented by numerical model experiments of Mississippi River plumes and Louisiana Coastal Currents, which is presented in section 5 for further interpretation of the observations.

2. Study Site and Observations

[7] Located in the southeast Louisiana, south of the city of New Orleans, Barataria Bay (Figure 1) is an irregularly shaped shallow estuary with a horizontal dimension of about $50 \times 50 \text{ km}$. It is bounded by the past and present Mississippi River ridges. The bay has several tidal inlets connecting with the coastal ocean of Louisiana Bight. Barataria Pass is one of these inlets between the Grand Isle and Grand Terre Island with a width of about 600 m. This is one of the main outlets of freshwater from the Barataria Basin. The main freshwater source of Barataria Bay is the Mississippi River water through the man-made Davis Pond Diversion facility, which has a capacity of about $250 \text{ m}^3/\text{s}$. The bay has an average depth of about 2 m. The main inlet (Barataria Pass) has a depth of slightly greater than 20 m. Inside the inlet there is a circular shaped depression of close to 50 m deep, according to our own observations using acoustic transducers.

[8] Beginning from the morning of 31 July and continuing to the morning of 1 August 2008 we conducted a 24 h continuous survey at the Barataria Pass aimed at determining the transport of water, suspended sediment, and nutrients. The observations were described by *Li et al.* [2009]. The focus of *Li et al.* [2009] was the intratidal variation of stratification due to tidal straining across the tidal inlet, which was an unexpected finding from the survey. In this paper, we focus on the original goal of the survey, the net transport of water and sediments. The transport of nutrient requires some detailed discussion of the biological and chemical processes and therefore will not be presented here.

[9] The observations and collections were done between 0630 LT on 31 July and 0610 LT on 1 August 2008. Tide in

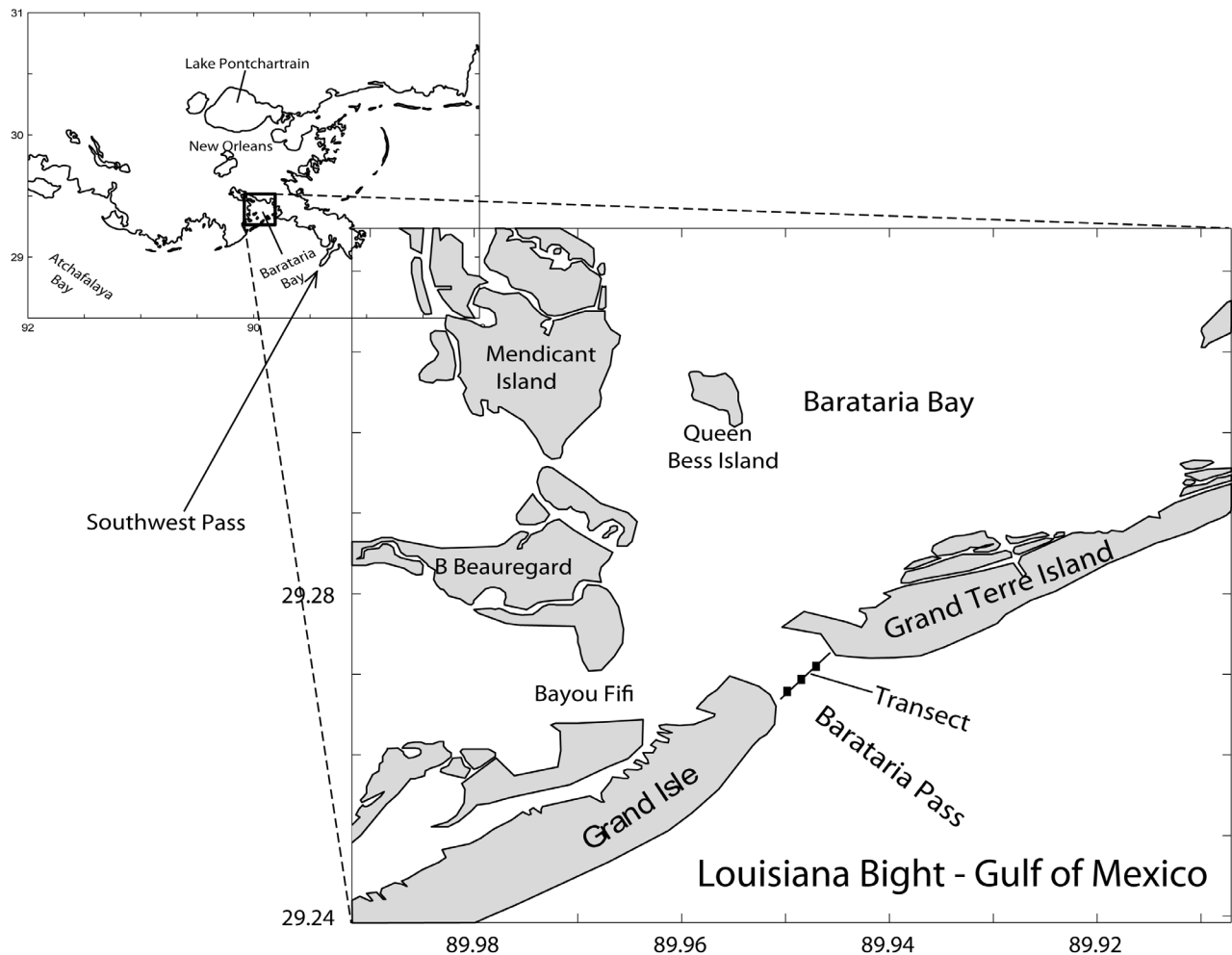


Figure 1. Map of study area. Shown here is the southeast Louisiana and Mississippi-Alabama coast. The Barataria Pass is shown with the transect and three CTD and water sample stations.

this area is microtidal. The maximum tidal range is only about 0.6 m. The dates of observations were selected to be at the spring tide, with close to the maximum tidal range (Figure 2a). Most of the variability of water level in this area is due to wind in winter time when cold front frequently occurs at 3–7 day intervals. In summer time, however, tidal oscillation usually dominates the water level variation. The wind during the survey was weak, averaged at less than 3 m/s (Figure 2b). This is a typical summer wind, except that localized short-term thunderstorms may have a significant increase in wind on a time scale of 1–2 h. A thunderstorm only occurred right after our survey on 1 August 2008. We used a 26 ft catamaran for the velocity measurements and water sampling. The boat was equipped with a Teledyne RD Instruments 600 kHz acoustic Doppler current profiler (ADCP), a Seabird Electronics thermosalinograph (SBE 45), and a Garmin GPS. A Seabird Electronics conductivity-temperature-depth sensor (CTD, SBE 19plus) integrated with a dissolved oxygen (DO) sensor (SBE 43), was also used for vertical profiles of water properties. The vertical profiles of the three dimensional velocity components (u , v , w) were measured almost continuously during the 24 h period. The transect was 530 m in length, occupying most of the 600 m

wide channel. The boat could not reach the very shallow waters (<1 m) for continuous observations without being grounded. Three stations were selected for CTD casts and water samples. They are located at $[-89.9475^{\circ}\text{W}, 29.2723^{\circ}\text{N}]$, $[-89.9484^{\circ}\text{W}, 29.2712^{\circ}\text{N}]$, and $[-89.9495^{\circ}\text{W}, 29.27^{\circ}\text{N}]$. A total of 28 CTD casts were made (Table 1). The salinity values ranged between 19 and 28.5 PSU with a maximum vertical salinity difference of about 5.5 PSU (See *Li et al.* [2009] for details of the hydrodynamic and hydrographic descriptions.) The nine sets of CTD casts were made almost evenly spread within the 24 h time period (Table 1) – each set includes a cast at each of the three stations except in the beginning when there was an extra cast at station S1 (Table 1).

3. Data Processing and Analysis

3.1. ADCP Data Analysis

[10] The ADCP data gave instantaneous profiles of velocity vectors at 2 Hz frequency at 0.5 m vertical intervals, excluding the near surface blanking distance (~ 1 m) below the depth of the ADCP transducers (~ 0.4 m below the surface). Since the boat occupied the transect line repeatedly at an average speed of less than 5 knots (2.5 m/s) over the

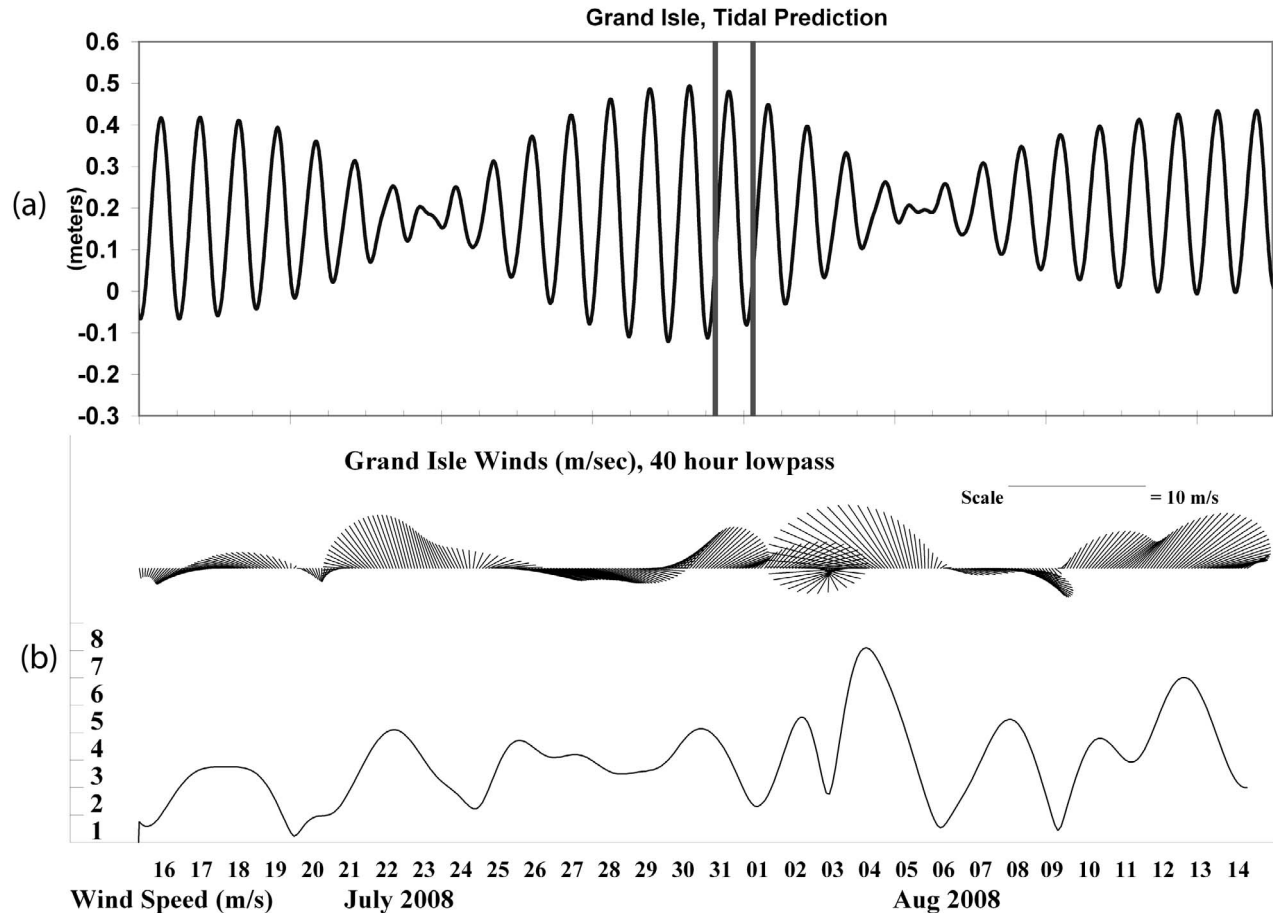


Figure 2. (a) NOAA predicted tide for the month before, during, and after the surveys. The start and end times of observations are indicated by the vertical lines. (b) Observed local wind vectors and magnitude at Grand Isle (only 40 h filtered results are shown).

24 h period, there were 122 replications. With this continuous and intensive survey, both temporal variations and spatial structures of the flow were captured.

[11] The ADCP data were first calibrated for misalignment and scaling as a standard procedure [e.g., Joyce, 1989]. We then rotated the coordinate system counterclockwise by 52.7° to have the along-channel and cross-channel velocity components. Only the along-channel velocity component is relevant to the transport in and out of the bay. A positive along-channel velocity (or transport) is defined to be toward the inside of the bay. The velocity vectors in the water column were then linearly interpolated in the interior and linearly extrapolated to the bottom and surface to obtain values at fixed vertical levels for ease of further analysis. Using nearest point value to replace linear extrapolation resulted in essentially the same result. For harmonic analysis of the tidal and subtidal constituents of the velocity, we divided the transect line into 29 segments and limited our selection of data points within 45 m upstream and 45 m downstream from the transect line [Li *et al.*, 2009]. We then regrouped all data points into these 29 locations. Each

location now has a time series of data points for all the vertical levels. We then applied a harmonic-statistic analysis [Li *et al.*, 2000; Li, 2002] to the along-channel velocity component. The only tidal constituents that we can reasonably include are diurnal and semidiurnal tides. Because of the short time series, we cannot distinguish among different species of diurnal or semidiurnal tides so we use $T = 24$ h for the diurnal group and $T = 12$ h for the semidiurnal group in the harmonic analysis.

3.2. Determination of Total Suspended Solids

[12] Water samples were collected six times during the 24 h observation period. At each time period, 1 L samples at three depths from each of the three stations: subsurface (1 m below surface), middepth, and 1 m above bottom were collected. The end of a 50 m long 0.01 m diameter polyethylene tubing was attached to the CTD proximal to the salinity sensor. By controlling the depth of the CTD, water samples from the three levels were collected by peristaltic pump at each station. The water samples were placed on ice and transported back to the lab where a measured volume of

Table 1. CTD Casts and Water Samples^a

| Cast | Date and Time (UTC) | Station | CTD Set | Water Sample | Time Used |
|------|---------------------|---------|---------|--------------|-----------|
| 1 | 31 Jul 2008 1149 | No data | | | |
| 2 | 31 Jul 2008 1155 | S1 | 1 | | 40 min |
| 3 | 31 Jul 2008 1209 | S1 | | 1 | |
| 4 | 31 Jul 2008 1225 | S2 | | 1 | |
| 5 | 31 Jul 2008 1235 | S3 | | 1 | |
| 6 | 31 Jul 2008 1453 | S1 | 2 | 2 | 15 min |
| 7 | 31 Jul 2008 1500 | S2 | | 2 | |
| 8 | 31 Jul 2008 1508 | S3 | | 2 | |
| 9 | 31 Jul 2008 1703 | S1 | 3 | | 13 min |
| 10 | 31 Jul 2008 1710 | S2 | | | |
| 11 | 31 Jul 2008 1716 | S3 | | | |
| 12 | 31 Jul 2008 1936 | S1 | 4 | 3 | 24 min |
| 13 | 31 Jul 2008 1947 | S3 | | 3 | |
| 14 | 31 Jul 2008 2000 | S2 | | 3 | |
| 15 | 31 Jul 2008 2157 | S1 | 5 | 4 | 28 min |
| 16 | 31 Jul 2008 2212 | S3 | | 4 | |
| 17 | 31 Jul 2008 2222 | No data | | | |
| 18 | 31 Jul 2008 2225 | S2 | | 4 | |
| 19 | 1 Aug 2008 0140 | S1 | 6 | 5 | 23 min |
| 20 | 1 Aug 2008 0154 | S3 | | 5 | |
| 21 | 1 Aug 2008 0203 | S2 | | 5 | |
| 22 | 1 Aug 2008 0445 | S1 | 7 | | 9 min |
| 23 | 1 Aug 2008 0449 | S2 | | | |
| 24 | 1 Aug 2008 0454 | S3 | | | |
| 25 | 1 Aug 2008 0743 | S1 | 8 | 6 | 22 min |
| 26 | 1 Aug 2008 0755 | S2 | | 6 | |
| 27 | 1 Aug 2008 0805 | S3 | | 6 | |
| 28 | 1 Aug 2008 1058 | S1 | 9 | | 8 min |
| 29 | 1 Aug 2008 1102 | S2 | | | |
| 30 | 1 Aug 2008 1106 | S3 | | | |

^aCTD longitude is $[-89.9475, -89.9484, -89.9495]$, and CTD latitude is $[29.2723, 29.2712, 29.27]$.

water was filtered through preashed glass fiber filters, dried at 105°C, and weighed to determine the total suspended solids (TSS). The filters were then ashed in a muffle furnace at 550°C for 4 h. The difference in weight between the pre and post burn indicate the amount of organic matter which was volatilized. This technique is widely used in wetlands, lakes, estuaries, bays, coastal waters, and wastewater treatment facilities [e.g., *White et al.*, 2009b; *Goñi et al.*, 2009; *Makarewicz et al.*, 2009; *Kayhanian et al.*, 2008; *Uthicke and Nobes*, 2008; *Nahlik and Mitsch*, 2008].

3.3. Transport Calculations

[13] To calculate the total transport of water and suspended sediment, we partitioned the vertical cross section into three smaller vertical sections centered at the three CTD stations each with 170 m in width. Each of these three subsections was then divided into three cells. With three water samples at each station, we have thus defined nine cells as shown in Figure 3a. By doing this we can obtain more accurate transport values using the areas as weight. The areas centered at S11, S12, and S13 are 250, 270, and 510 m², respectively. The areas centered at S21, S22, and S23 are 920, 1190, and 850 m², respectively. The areas centered at S31, S32, and S33 are 770, 840, and 850 m², respectively (Figure 3a).

[14] The time series data of the concentrations have irregular time intervals (Table 1). We interpolated the time series of concentrations onto equally spaced (hourly) data using Spline Functions and allowing extrapolation at the end

point before calculating the total transport. The use of six samples over a tidal cycle is limited. But the sampling of six times still stretched to the limit that we could do given space and time. The interpolation aids in making the calculation of transport easier but the error is not easy to quantify as we have no reference to compare. Unless we do a much higher-resolution experiment, we cannot estimate the error. However, the interpolated data do seem to be quite consistent and therefore should provide a reasonable representation. The transport of TSS at each of the hourly time instances was done by the multiplication of TSS concentration, area of the cell of consideration, and the averaged along-channel velocity within the cell at the time of observations. We used the observed velocity values for the calculations, not those from the harmonic fit. The total transport at given time was then obtained by adding the transport for each of the nine cells.

4. Observational Results

4.1. Velocity Field

[15] Figure 3a shows the vertical profiles of the color filled contours of amplitude of the diurnal along-channel tidal velocity. Shown in Figure 3a are also three locations of the CTD casts and nine vertical locations of water samples. It can be seen that velocity magnitude is highest in the center of the channel where it has the deepest water which has a maximum of 1.3 m/s. The near bottom velocity magnitude is smaller than that near the surface due to bottom friction. This is a typical result for frictional tidal currents in channels as shown by observations [*Li et al.*, 1998, 2004], 2-D models [*Li and Valle-Levinson*, 1999], and 3-D models [*Li*, 2001]. The semidiurnal tidal constituent is very small and cannot be discerned from the noise and errors. This is because the area is dominated by diurnal tides. Therefore, the semidiurnal tidal component is insignificant and not meaningful for further discussion in this case.

[16] Figure 3b shows the mean (subtidal) along-channel velocity. Positive values are defined to be into the bay. There are a few characteristics need to be noted. First, the majority of the flow is going outward with the maximum reaching ~0.5 m/s on the western end of the transect. Second, there is a weak inward flux concentrated at the bottom of the deep water. The maximum inward net velocity at bottom is about 0.05 m/s, an order of magnitude smaller than the outward flows which are mostly concentrated on the surface and on the two sides with shallower waters. This is a typical estuarine circulation across a triangular shaped cross section as shown by models and observations [e.g., *Wong*, 1994]. This type of exchange flow is also the same as tidally induced flow in a short channel with standing tidal wave characteristics [*Li and O'Donnell*, 2005]. The relatively weak net outward flow on the eastern end of the inlet coincides with the relatively lower salinity on that end [*Li et al.*, 2009], suggesting a possible source of low-salinity water from outside of the bay that came in more from the eastern end, reducing the outward flow more on the east. This is a new feature that the conventional estuarine circulation does not usually consider, to which we will discuss more with a numerical model experiment in the following.

[17] To assess the quality of the representation of tidal harmonic components and a mean flow, the R² values of the

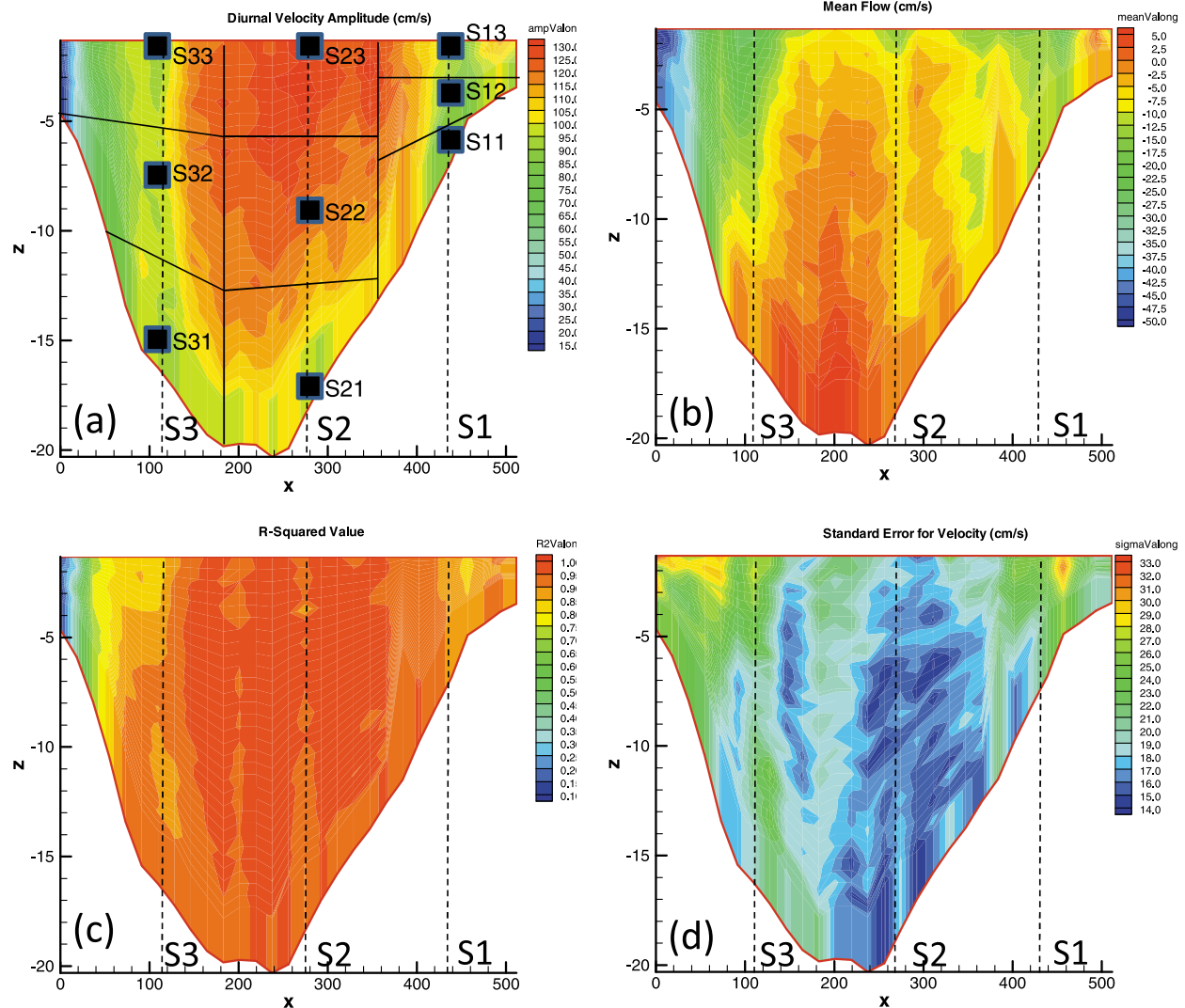


Figure 3. Cross-sectional views of (a) along-channel tidal velocity amplitude (cm/s) from harmonic analysis, (b) tidally averaged flow velocity (cm/s), (c) R^2 values of the harmonic analysis, and (d) standard error of the harmonic analysis (cm/s). The left side is the west side.

harmonic fit are calculated as shown in Figure 3c. It is apparent that most of the positions have R^2 values very close to 1. However, the R^2 values tend to decrease toward shallower waters on both sides of the transect. This is very clear on the western end where the R^2 values are less than 0.3. Similarly, the standard error of the data from the harmonic fit shown in Figure 3d has relatively small values in the channel than on the sides of the inlet where the standard error can reach ~ 0.3 m/s. This is caused by nonharmonic and nontidal variations of transient local eddies near the barrier islands particularly on the west end of the transect that we observed during the survey. As observed in Vermilion Bay by *Li and Weeks* [2009], small eddies on the order of a few hundred meters in diameter in tidal inlets with complex bathymetry and topography can form. Figure 4 shows some examples of such eddies on the western end

of the transect. The dash-dotted line of Figure 4 shows the northeast-southwest oriented transect. The eddy was rotating counterclockwise, in contrast to the eddy observed by *Li and Weeks* [2009] with clockwise rotation. What is shown in Figures 4a and 4b are actually the same eddy measured twice in about 10 min and this eddy lasted for at least 2 h. It can be seen that the diameter is more than 100 m and is evolving over time. The transient nature of the eddy apparently causes the low R^2 values in the harmonic analysis. This eddy is apparently associated with the barrier island and bathymetry and is thus a headland eddy. Its position and sense of rotation changed when tidal current reversed. We omit more detailed discussion of the eddy. This also indicates that transports through tidal inlets is strongly influenced by the eddy and we need to have a time series of velocity to accurately calculate the total flux

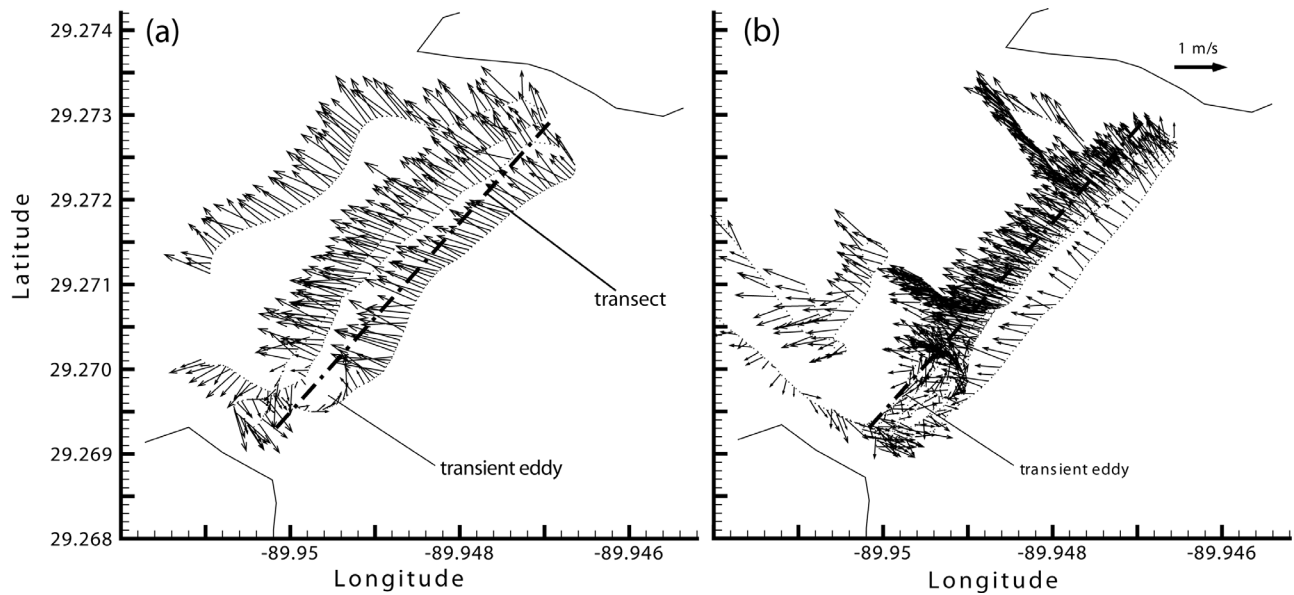


Figure 4. Examples of velocity vectors showing some transient eddies at the western end of the transect during flood stage. The velocity is from subsurface, 1.32 m below the surface. Shown for observation times (a) 1432–1450 and (b) 1450–1632 UT.

(integrated across the transect) and net flux (mean total flux).

4.2. Time Series of TSS Concentrations

[18] Figure 5 shows the time series of TSS concentrations at the three stations and three vertical levels. Obviously, during this observational period the TSS concentration shows different temporal variations at each station and each level. At the northeast end of the transect (station S1), the bottom TSS was high (>400 mg/L) in the beginning of the survey when it was flooding (Figure 6a), but it subsequently dropped quickly and never rebounded substantially (Figure 5a). As anticipated, the bottom TSS was always larger than that at the middepth; while the near surface concentration was the smallest.

[19] This relatively large input of TSS from the northeast end of the transect during flood from outside of the bay is consistent with the observed fresher water on the northeast end in the beginning of the survey [Li *et al.*, 2009, Figure 6]. This is also supported by a larger stratification on the northeast end in the beginning of the survey [Li *et al.*, 2009]. It was speculated by Li *et al.* [2009] that a coastal current from the outside of the bay influenced by the freshwater from the Southwest Pass of the Mississippi River Delta might have come through either the Louisiana Coastal Current or a recirculation of an anticyclonic gyre as observed by remote sensing [Rouse and Coleman, 1976; Walker *et al.*, 2005] and in situ observations [Murray, 1998].

[20] In contrast, the southwest end of the transect started with low TSS concentrations at all depth. This is also consistent with the observations of an eddy rotating counter-clockwise which had an outward flow on the southwest end. This counter current (during flood tide) was against the incoming shelf water. The TSS concentration at the south-

west end remained high (Figure 5c) for the rest of the time period. The middle station S2 had a relatively low TSS concentration most of the time except during peak ebb when the values increased (Figure 5b). The difference in TSS concentration between the northeast and southwest ends is anticipated as the stratification across the transect had an out-of-phase oscillation as discussed in detail by Li *et al.* [2009].

[21] The rate of integrated transport of water is more regular and has a sinusoidal pattern (Figure 6a). The total rate of transport during peak flood is more than 6000 m³/s and close to 8000 m³/s during peak ebb; thus a net outward flux. The northeast 1/3 of the section has the smallest magnitude and the central 1/3 of the transect has the largest magnitude because of the shallow water on the northeast end and deep water in the center of the channel (Figure 3). The rate of transport of water through the southwestern 1/3 of the section is between those of the other two 1/3 sections.

[22] The rate of transport of TSS is less regular and demonstrates some nonsinusoidal variations (Figure 6b) compared to that of water (Figure 6a). The west, east, and central sections are not in phase for TSS transport. During the peak flood the maximum inward TSS flux is 800 kg/s while the maximum outward TSS flux is 900 kg/s. The southwest 1/3 of the section appears to have a disproportionately larger TSS flux compared to the central 1/3. Within the TSS, a large fraction is inorganic (Figure 6c). The west and east/central are not in phase.

[23] The TSS is composed of $\sim 81\%$ of inorganic material with the remaining composed of organic material. Consequently, there is a much larger flux of inorganic material out of the bay (Figure 6c) compared to organic matter (Figure 6d) and this is consistent with the organic matter content of the Louisiana shelf sediments [White *et al.*, 2009a].

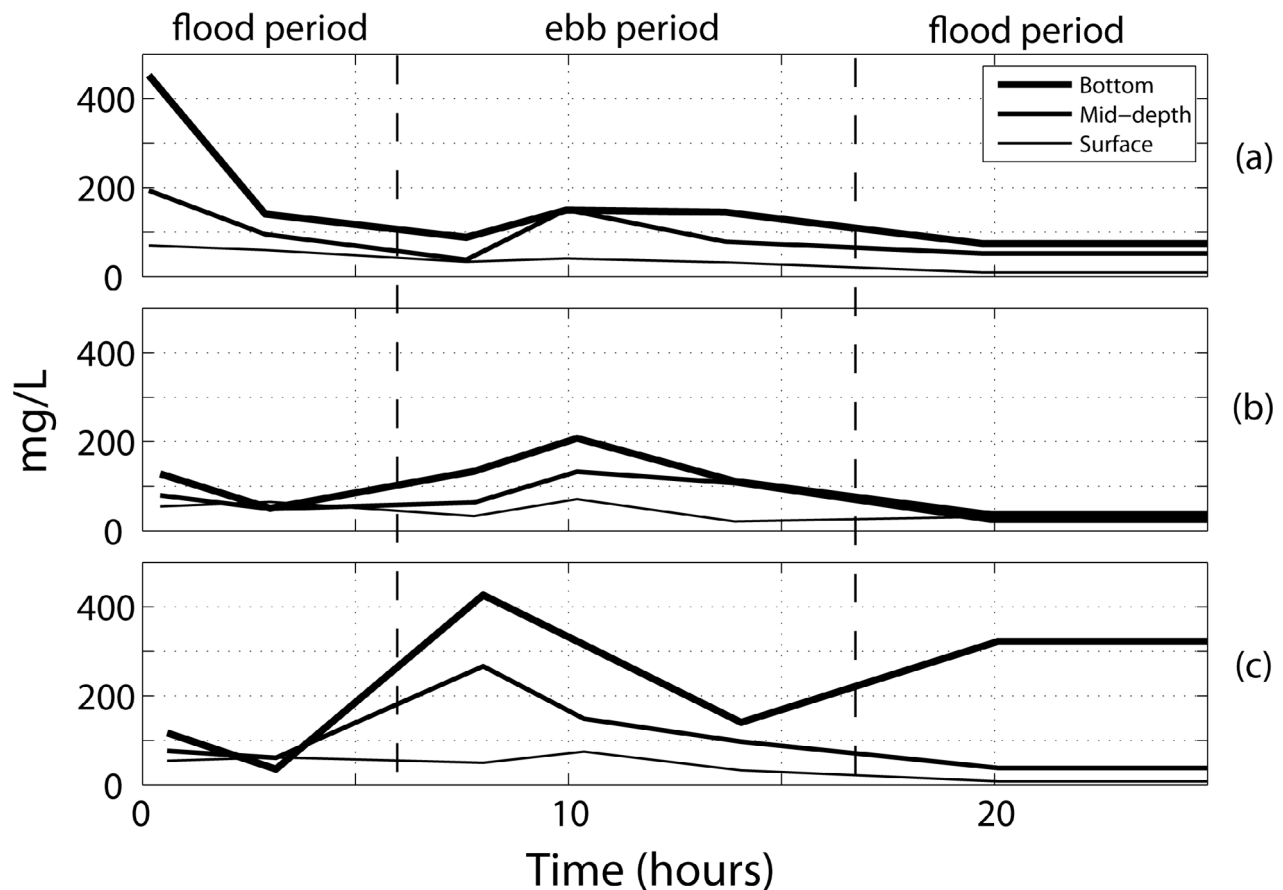


Figure 5. Time series of total suspended solid (TSS) concentration (mg/L) at the three stations (Figure 1). Data corresponding to stations (a) 1, (b) 2, and (c) 3 are shown as well as three different depths (bottom, middepth, and near surface).

4.3. Net Transport

[24] The net water flux is calculated to be 27 million t within the 24 h period (Table 2). The averaged outward rate of flux is thus about $380 \text{ m}^3/\text{s}$ (Table 2). Considering the total volume of the Barataria Bay of 633 million m^3 [Feng and Li, 2010], the flushing time would be about 19 days. If we assume that the flux going through Barataria Pass accounts for 66% of the total [Marmor, 1948], then flushing time should be modified to about 13 days. Considering the change of bathymetry (dredging in Barataria Pass), the flushing time of the bay should be between 19 and 13 days. Comparing with the model estimate of 15 days [Inoue et al., 2008], this result appears to be reasonable. The net transport of TSS was ~ 8.8 thousand t during the 24 h period, of which ~ 7.16 thousand t were from inorganic suspended solids. There was a net flux of 1.64 thousand t of particulate organic matter transported from the semienclosed bay to the coastal ocean. Upon inspection under compound microscope, much of this material was detrital material derived from the coastal marshes that line the bay. These findings however are for normal weather conditions in the summer. In winter times, the flushing rate can be significantly higher and half of the bay can be emptied within a day or two [Feng and Li, 2010]. The winter time flushing rate is apparently similar for the major Louisiana bays: Barataria

Bay, Atchafalaya Bay, Vermilion Bay, Timalier Bay, and Terrebonne Bay [Feng and Li, 2010]. Our study for the summer condition so far is limited to Barataria Bay only.

5. Discussion

5.1. Discussion of the Observations

[25] The observations have shown a few interesting features of the fluxes of water and suspended sediments. One of these features is the difference between the first flood period (time < 5 h) and the second flood period during the survey (time > 17 h). The relatively stronger influx of suspended sediment on the eastern end during the first few hours of the survey was coincident with the relatively fresher water and a strong stratification on the eastern end at that time [see Li et al., 2009, Figures 5a and 6]. This influx of relatively fresher water on the eastern end was not repeated during the second flood period, indicating that it was just a transient process influenced by the tide and shelf circulation which may have entrained some of the freshwater from the Mississippi River mouth into the coastal water. This is an assumption that led to the numerical experiments (see below).

[26] Another feature is the difference between the western and eastern ends. This is consistent with the results of Li et al. [2009], in which it is concluded that there was a much larger

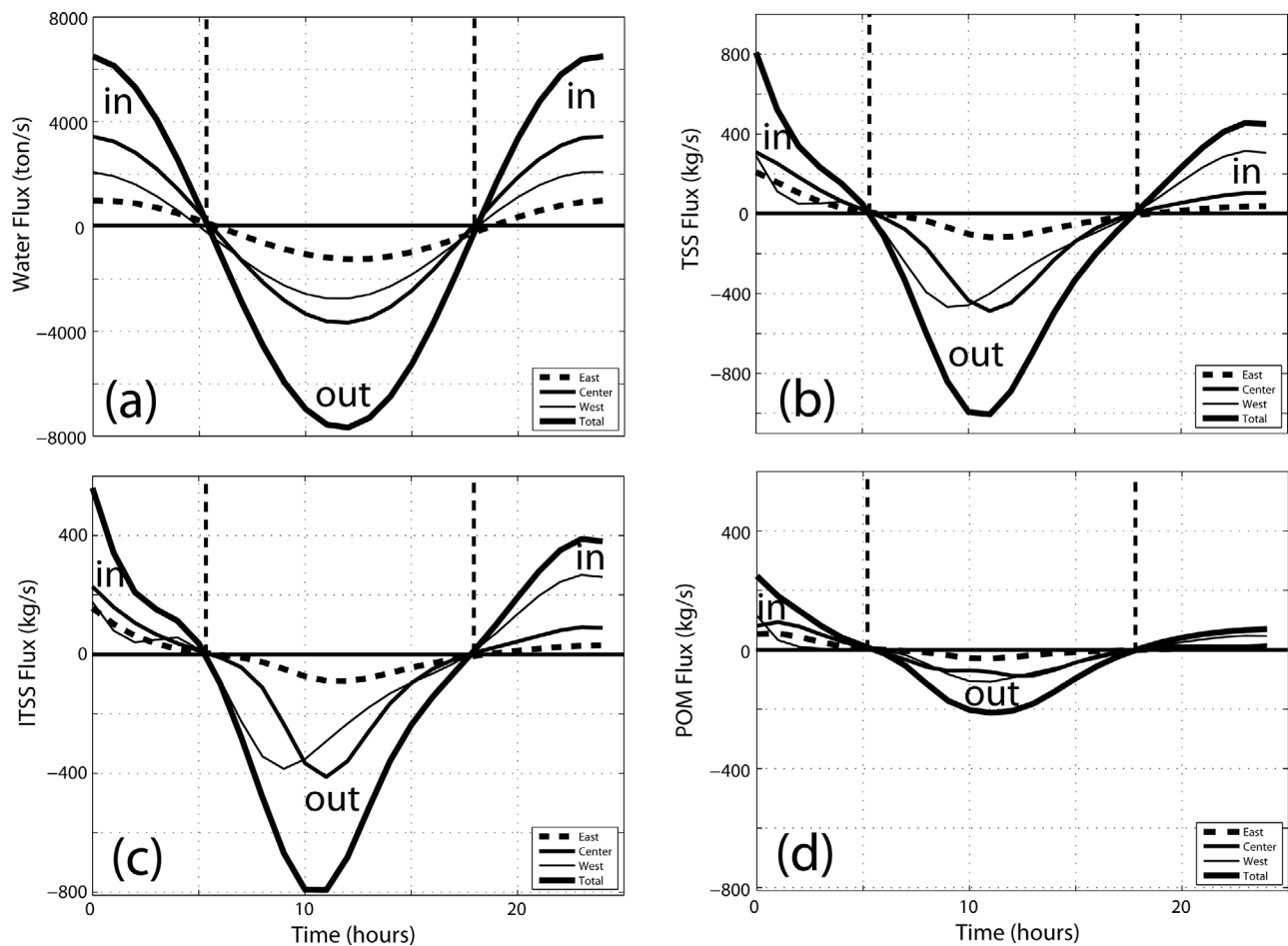


Figure 6. Time series of (a) water flux (t/s), (b) TSS flux (kg/s), (c) inorganic TSS flux, and (d) particulate organic matter.

uncertainty over the banks, suggesting a stronger nonlinearity near the edges of the barrier islands on both sides of the channel. It was also found in the earlier study that there was a lateral variation and inversion of the Average Potential Energy Demand (APED) which was a result of differential tidal straining across the tidal channel [Li *et al.*, 2009]. This lateral asymmetry is in contrast to the temporal asymmetry that has been most studied [e.g., Simpson *et al.*, 1990, 2005; Rippeth *et al.*, 2001; Geyer *et al.*, 2000; Chant and Stoner, 2001; Stacey and Ralston, 2005; Ralston and Stacey, 2007; Li and Zhong, 2009]. Related to that finding is the nonuniform distribution of the surface salinity which had a larger mean value on the western end than much of the eastern end, contrary to the expected situation in an estuary where a larger mean surface salinity is produced on the eastern (opposite) end due to Coriolis force. In the beginning of the survey, the eastern side had more than twice as large of the APED as that of the western side; while toward the end of the survey (close to the second maximum flood), the western side had an APED more than 6 times of that of the eastern side. Li *et al.* [2009] suggested that this lateral difference in APED indicated that there must be other factors influencing the stratification and altering the tidal straining. An example is a relatively fresher water plume entering the bay. This relatively fresher water (compared to the average shelf water in the area) may come

from the river plume of the Southwest Pass of Mississippi River Bird's Foot Delta. This hypothesis was tested next with our numerical experiments.

[27] The observations also demonstrate eddies near both ends especially the western end. These eddies are results of nonlinearity and they impact the net transport. However, due to the small scale (100–150 m in diameter), the precise impact to the transport cannot be easily quantified, we only have three stations for water samples across the 530 m transect. Adding more water sample stations may not be practical because of the strong currents during much of the tidal period, busy boat traffic, and overnight operations. Nevertheless, the velocity profiles were continuously measured, with a spatial resolution of about 18 m for the processed data (29 segments within 530 m).

Table 2. Total Mass Flux Through Barataria Pass^a

| Substance | Net Quantity (t) |
|------------------------------------|--------------------------------------|
| H ₂ O (Water flux rate) | -2.7394e+007 (380 m ³ /s) |
| TSS | -8.8040e+003 |
| Inorganic TSS | -7.1576e+003 |

^aBarataria Bay volume is 6.33×10^8 m³, and residence time is V/R = 19 days.

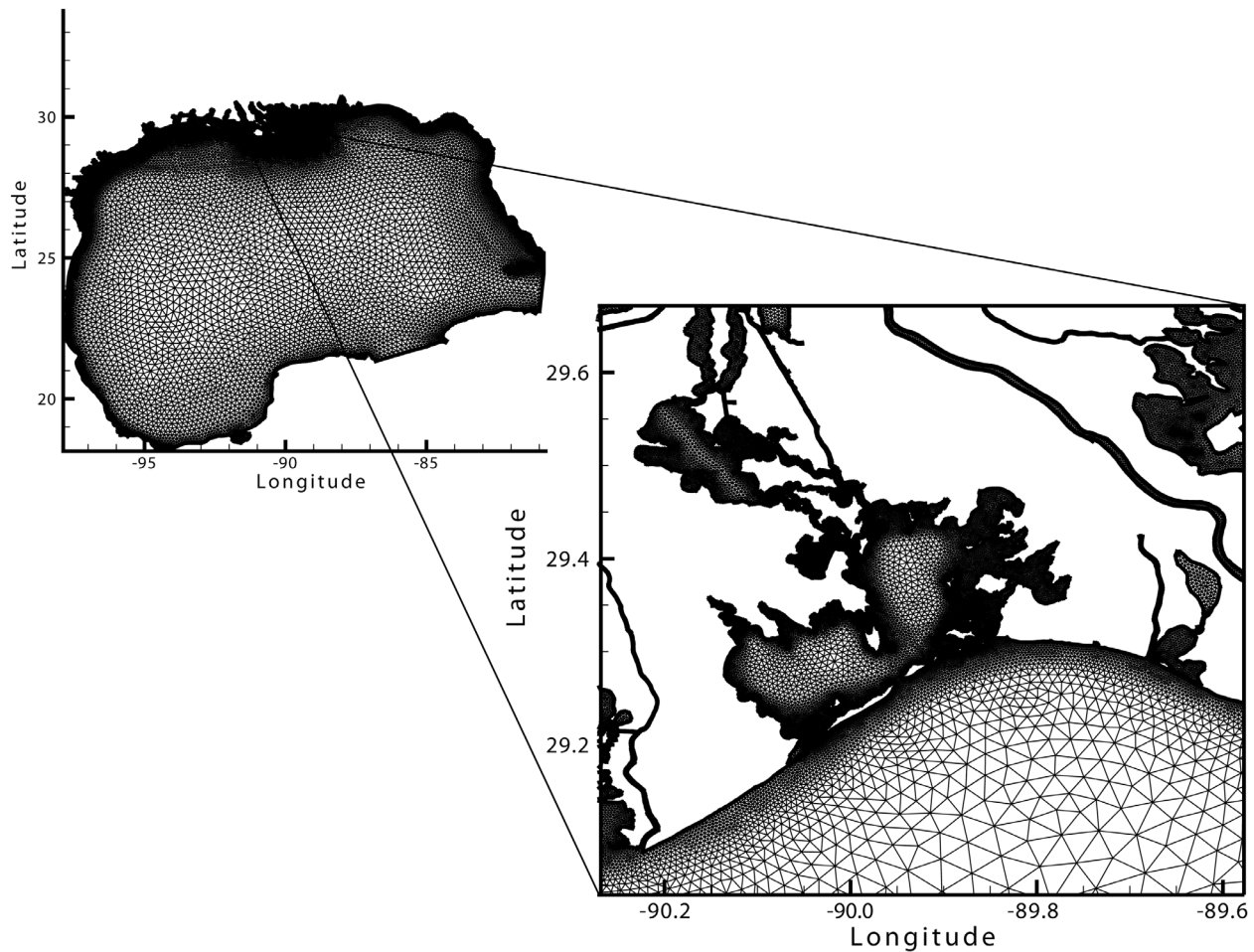


Figure 7. Finite Volume Coastal Ocean Model grid.

[28] To verify our hypothesis that Mississippi River water can enter into the Barataria Bay and to demonstrate the local small-scale transient eddies, we have conducted some process oriented numerical experiments, which are discussed below.

5.2. Numerical Model Experiments

[29] In the process oriented numerical model experiments, we applied the Finite Volume Coastal Ocean Model (FVCOM) [Chen *et al.*, 2003] to the entire Gulf of Mexico with a particular focus on the northern coastal area. FVCOM has been applied to this area in several studies for storm surge [e.g., Rego and Li, 2010a, 2010b, 2009a, 2009b], tidally induced eddies in curved channels [Li *et al.*, 2008], and factors influencing the seasonal hypoxia [Wang and Justic, 2009].

[30] In the present work, we implemented the FVCOM to the entire Gulf of Mexico with a focus on the study area of the northern coast with a fine spatial resolution (the finest grid size is ~ 20 m) and the model domain covers all the bays and estuaries and major waterways along the Louisiana coast. As shown in Figure 7, the Barataria Bay is covered with high-resolution triangular grids. Freshwater discharges from 12 rivers were included in the numerical simulation

aimed at the resolution of the Mississippi River plume and associated Louisiana Coastal Current. The model has two open boundaries as shown in Figure 7: the Strait of Florida and the Yucatan Channel. Tide from an FVCOM global ocean model of the University of Massachusetts at Dartmouth was used for the open boundary conditions. Tide-generating potential was also applied in the Gulf of Mexico for forced tides. The model includes 264,228 triangular elements and 161,307 nodes. A semi-implicit version of FVCOM is used with a time step of 4 s. An 11-level sigma coordinate was used for the vertical. The model was run for an averaged spring condition with 12 rivers, aimed at a study on the process and the examination of the coastal current resulted from the Mississippi River and possible intrusion of the low-salinity water into the Barataria Bay. Figure 8 shows a snap shot of the surface current velocity vectors which indicates the circulation around the Bird's Foot Delta and Louisiana Bight as well as the coastal current along the coast outside of the Barataria Bay (roughly east to west). The surface salinity distribution is shown in Figure 9 which clearly demonstrates a relatively low-salinity coastal water entering the Barataria Bay. To further verify the model results we conducted a vessel-based survey on 5 May 2010 using an ADCP mounted on a 26 ft catamaran. During this

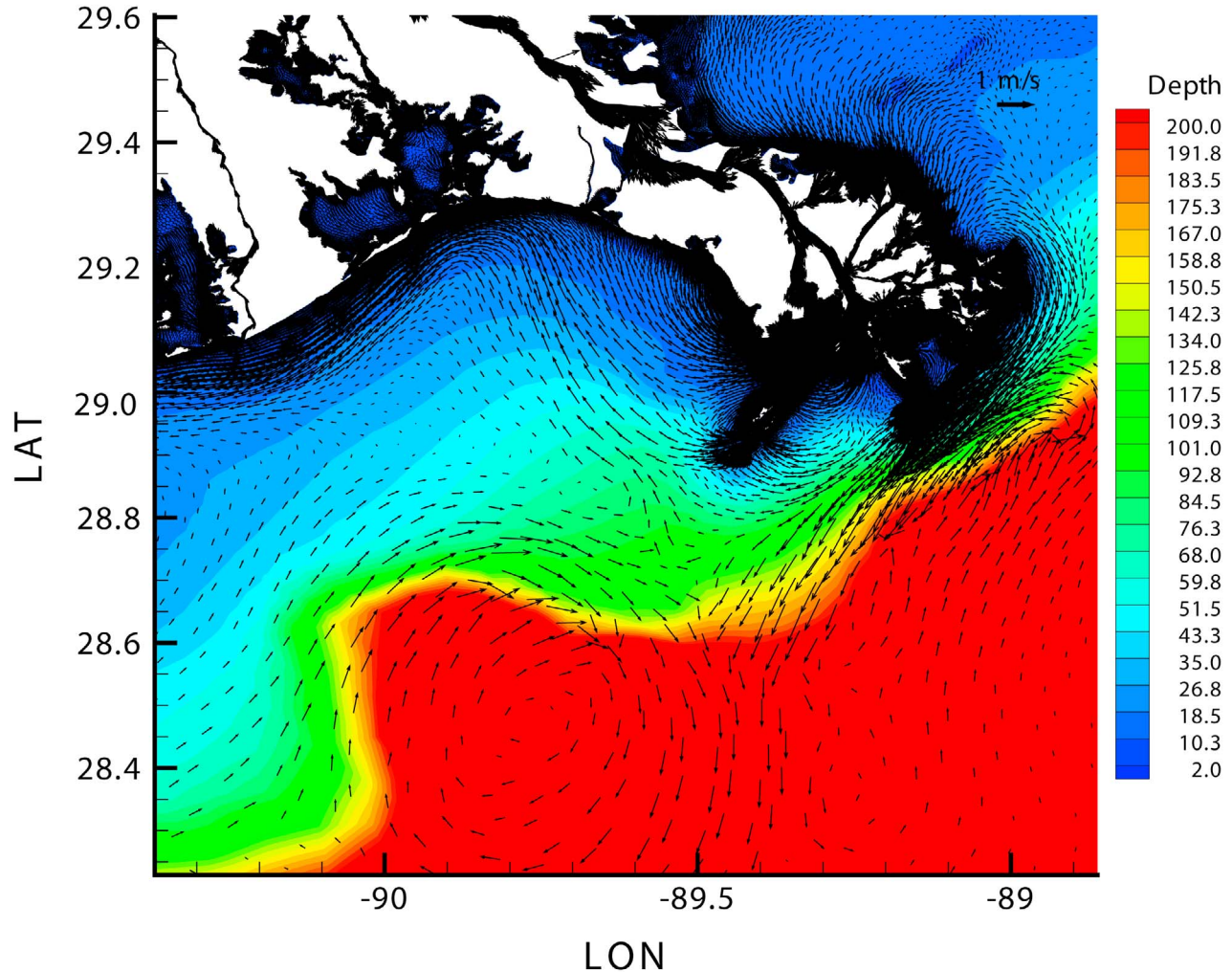


Figure 8. A typical surface current pattern from the numerical experiments.

survey, we used the same vessel and ADCP as we did during the 2008 survey at the Barataria Pass. The data presented here (Figure 10) is the near surface (~ 2 m below the surface) flow vectors measured from 1903:54 to 2048:44 UTC. The comparison of surface current between the model and observations are remarkably well (Figure 10). This provides confidence to the model results of coastal current entering into Barataria Bay.

6. Summary

[31] In this study, a 24 h continuous survey of hydrodynamics and water sampling have allowed us to calculate the intratidal variations of fluxes and net transport of water and suspended sediments through the Barataria Pass, the major tidal inlet of the Barataria Bay. The tidal velocity amplitude shows a stronger magnitude on the surface in the center of the channel which decreases toward the banks, a condition of frictional tide. The flow field is observed to have transient eddies at the edges of the barrier islands, which causes low R^2 values of the harmonic fit at the edges of the inlet. The

net outward flow is through the surface and both sides of the inlet, with a maximum reaching 0.5 m/s. Only a small magnitude (0.05 m/s) of net inward flow occurs near the bottom in deep water. This distribution of net flow field is typical in an estuary with a triangular cross section [Wong, 1994]. This is also a pattern consistent with tidally induced exchange flow in a short estuary with a triangular cross section [Li and O'Donnell, 2005], even though the tidally induced flow is from an entirely different mechanism in a barotropic environment. The west side however shows a much larger outward flow than the east side. This is coincident with a fresher east side, which suggests that the Louisiana Coastal Current around the Birdfoot delta derived from the mixing of shelf water with the Mississippi River freshwater may have entered the Bay, mostly from the east side during the survey, which results in a smaller outward flow on the eastern side.

[32] The net flux of water is calculated to be $380 \text{ m}^3/\text{s}$ with a total of 27 million t in weight in 24 h period which results in an estimate of the flushing time for the Barataria Bay to be 13–19 days. The total flux of suspended solid is

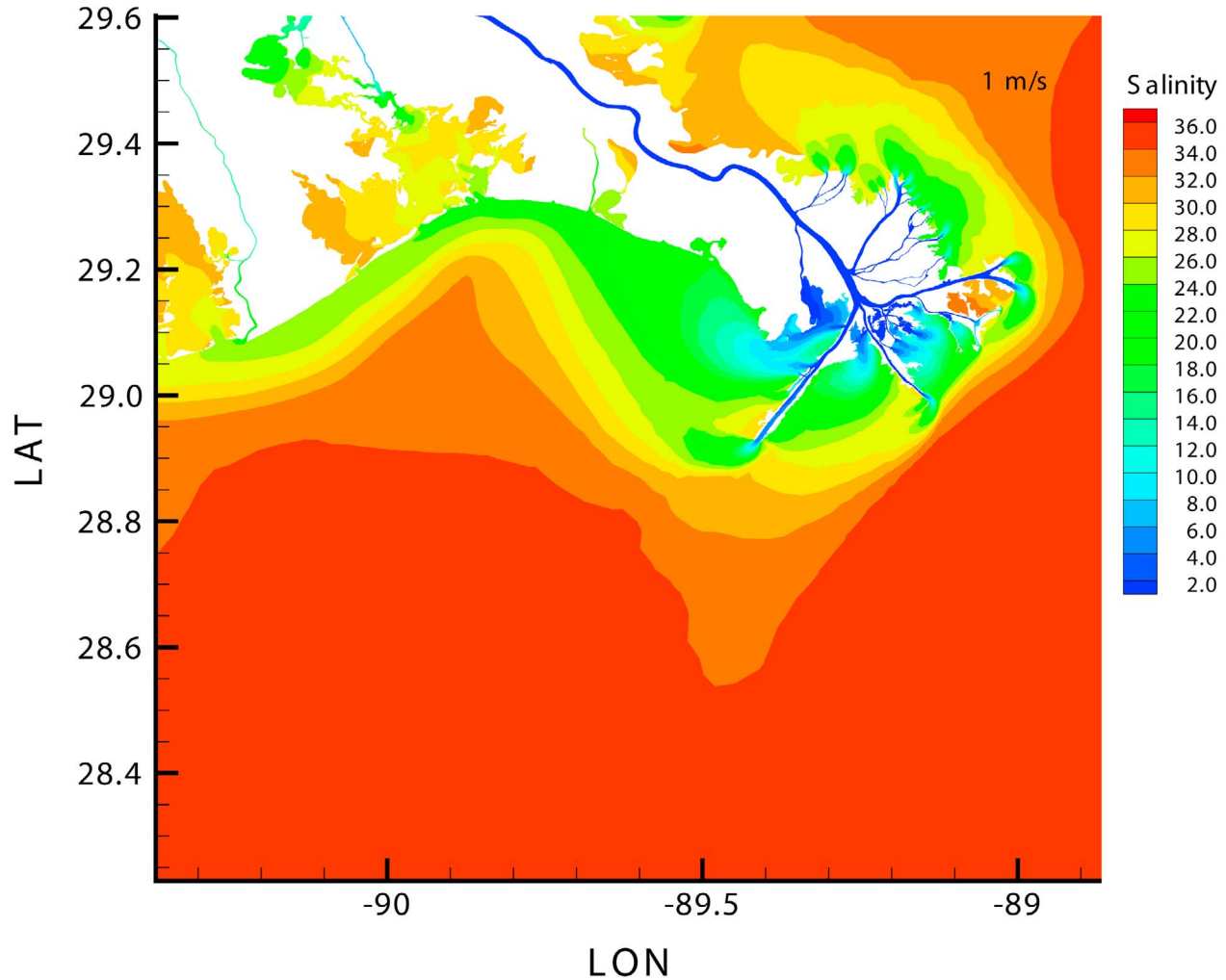


Figure 9. A typical surface distribution of salinity.

estimated to be ~9000 t, of which 80% was inorganic suspended sediment. A process-oriented numerical model simulation using a high-resolution Finite Volume Coastal Ocean Model (FVCOM) shows that relatively fresh water can intrude into Barataria Bay through the inlets as a result of the expansion of the Mississippi River plume and Louisiana Coastal Current, supporting the hypothesis that river water may come from outside of the bay, further confirming our finding of an abnormal stratification variation across the inlet in a earlier publication on asymmetry of tidal straining [Li *et al.*, 2009]. The model is verified by field observations on 5 May 2010.

[33] The physical processes that affect the magnitude of velocity, vertical mixing and stratification, and bottom turbulence, also affect the suspended sediment transport. The study presented here is for typical summer conditions in which wind is weak and stratification more pronounced as the weak vertical mixing due to lack of wind stirring coincides with strong surface heating. As mentioned earlier, Barataria Bay water interacts with the Louisiana shelf water,

which is in turn influenced by the Mississippi River water. Outside of the Bay is the world second largest hypoxia zone, occurring in the summer, second only to that in the Baltic Sea. Southern Louisiana is also well known for its rapid rate of land loss. With 30% of the coastal marsh area, Louisiana accounts for 90% of its loss [Dahl, 2000]. All these highlight the importance of the flushing of the bays and the suspended sediment transport between Louisiana bays and the Louisiana shelf. The flushing of the Louisiana bays in the winter is largely controlled by cold fronts formed by large-scale weather systems that occur at 3–7 day intervals [Roberts *et al.*, 1989; Walker and Hammack, 2000; Feng and Li, 2010; Li *et al.*, 2011]. This study provides the most detailed sample over a 24 h period for this system, quantifying the rate of flushing (or residence time) and the net transport of water and sediments. The data will be useful for model validation for studying the flushing process of the Louisiana bays. In addition, the finding of this study about the intrusion of Mississippi River water into the bay through the eastern side of the channel implies more complex

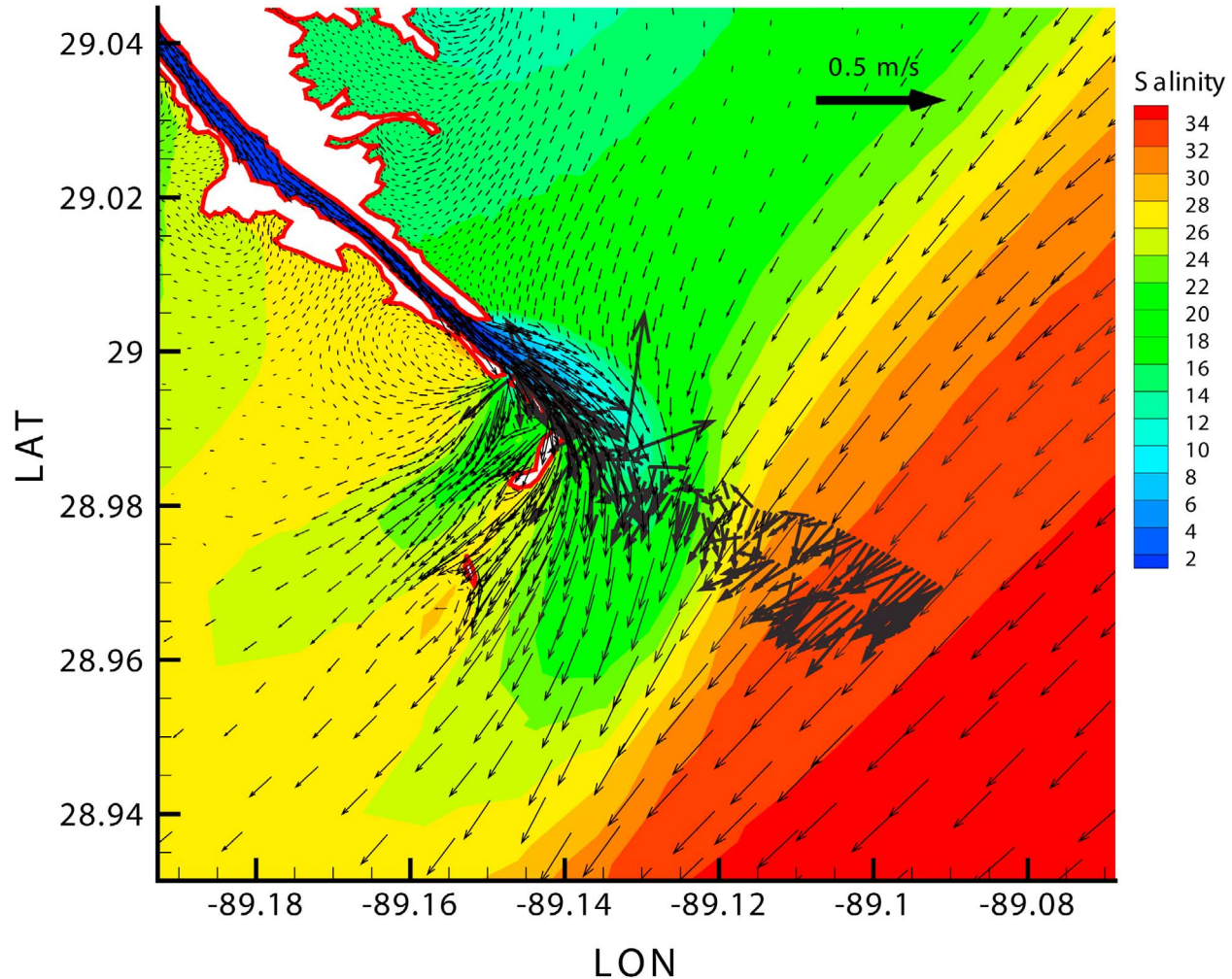


Figure 10. Comparison of model results (thin arrows) and observed surface currents (thick arrows) on 5 May 2010.

interaction between the bay and shelf waters. Obviously, the details of the dynamics of this interaction are yet to be fully explored. Our study provides more motivation for further studies and more questions than answers.

[34] **Acknowledgments.** The research was supported by NSF (DEB-0833225), and two NOAA grants, NA06NPS4780197 for NGoMEX funded to LUMCON and LSU and NA06OAR4320264–06111039 to the Northern Gulf Institute by NOAA's Office of Ocean and Atmospheric Research, the U.S. Department of Commerce, and Shell (<http://www.ngi.lsu.edu/>). The work is also partially supported by the Shanghai Ocean University Program for International Cooperation (A-2302-10-0003) and the Program of Science and Technology Commission of Shanghai Municipality (09320503700). We would particularly like to thank Charlie Sibley, Chris Cleaver, Darren Depew, Steve Jones, and Rodney Fredericks for the field work. We appreciate the detailed comments by two anonymous reviewers that resulted in the improvement of the paper.

References

- Benke, A. C., and C. E. Cushing (2005), *Rivers of North America*, 1144 pp., Elsevier, San Diego, Calif.
- Chant, R. J., and A. W. Stoner (2001), Particle trapping in a stratified flood-dominated estuary, *J. Mar. Res.*, *59*, 29–51, doi:10.1357/002224001321237353.
- Chen, C., H. Liu, and R. Beardsley (2003), An unstructured grid, finite-volume, three-dimensional, primitive equations ocean model: Application to coastal ocean and estuaries, *J. Atmos. Oceanic Technol.*, *20*, 159–186, doi:10.1175/1520-0426(2003)020<0159:AUGFVT>2.0.CO;2.
- Dahl, T. E. (2000), Status and trends of wetlands in the conterminous United States 1986 to 1997, report, 84 pp., U. S. Dep. of the Inter., Fish and Wildl., Washington, D. C.
- Feng, Z., and C. Li (2010), Cold-front-induced flushing of the Louisiana bays, *J. Mar. Syst.*, *82*, 252–264, doi:10.1016/j.jmarsys.2010.05.015.
- Geyer, W. R., J. H. Trowbridge, and M. M. Bowen (2000), The dynamics of a partially mixed estuary, *J. Phys. Oceanogr.*, *30*, 2035–2048.
- Goñi, M. A., G. Voulgaris, and Y. H. Kim (2009), Composition and fluxes of particulate organic matter in a temperate estuary (Winyah Bay, South Carolina, USA) under contrasting physical forcings, *Estuarine Coastal Shelf Sci.*, *85*, 273–291, doi:10.1016/j.ecss.2009.08.013.
- Inoue, M., and W. J. Wiseman Jr. (2000), Transport, mixing and stirring processes in a Louisiana estuary, *Estuarine Coastal Shelf Sci.*, *50*, 449–466, doi:10.1006/ecss.2000.0587.
- Inoue, M., D. Park, D. Justic, and W. J. Wiseman Jr. (2008), A high-resolution integrated hydrology-hydrodynamic model of the Barataria Basin system, *Environ. Model. Softw.*, *23*, 1122–1132, doi:10.1016/j.envsoft.2008.02.011.
- Joyce, T. M. (1989), On in situ calibration of shipboard ADCPs, *J. Atmos. Oceanic Technol.*, *6*, 169–172, doi:10.1175/1520-0426(1989)006<0169:OISOSA>2.0.CO;2.
- Justic, D., V. J. Bierman Jr., D. Scavia, and R. D. Hetland (2007), Forecasting Gulf's hypoxia: The next 50 years?, *Estuaries Coasts*, *30*, 791–801.

- Kantha, L. (2005), Barotropic tides in the Gulf of Mexico, in *Circulation in the Gulf of Mexico: Observations and Models*, *Geophys. Monogr. Ser.*, vol. 161, edited by W. Sturges and A. Lugo-Fernandez, pp. 159–163, AGU, Washington, D. C.
- Kayhanian, M., E. Rasa, A. Vichare, and J. E. Leatherbarrow (2008), Utility of suspended solid measurements for storm-water runoff treatment, *J. Environ. Eng.*, *134*, 712–721, doi:10.1061/(ASCE)0733-9372(2008)134:9(712).
- Kjerfve, B. (1978), Bathymetry as an indicator of net circulation in well-mixed estuaries, *Limnol. Oceanogr.*, *23*, 816–821, doi:10.4319/lo.1978.23.4.0816.
- Kjerfve, B., L. H. Stevenson, J. A. Proehl, and T. H. Chrzanowski (1981), Estimation of material fluxes in an estuarine cross section: A critical analysis of spatial measurement density and errors, *Limnol. Oceanogr.*, *26*, 325–335, doi:10.4319/lo.1981.26.2.0325.
- Li, C. (2001), 3D analytic model for testing numerical tidal models, *J. Hydraul. Eng.*, *127*, 709–717, doi:10.1061/(ASCE)0733-9429(2001)127:9(709).
- Li, C. (2002), Axial convergence fronts in a barotropic tidal inlet—Sand shoal inlet, VA, *Cont. Shelf Res.*, *22*, 2633–2653, doi:10.1016/S0278-4343(02)00118-8.
- Li, C., and J. O'Donnell (2005), The effect of channel length on the residual circulation in tidally dominated channels, *J. Phys. Oceanogr.*, *35*, 1826–1840, doi:10.1175/JPO2804.1.
- Li, C., and A. Valle-Levinson (1999), A two-dimensional analytic tidal model for a narrow estuary of arbitrary lateral depth variation: The intratidal motion, *J. Geophys. Res.*, *104*, 23,525–23,543, doi:10.1029/1999JC900172.
- Li, C., and E. Weeks (2009), Measurements of a small scale eddy at a tidal inlet using an unmanned automated boat, *J. Mar. Syst.*, *75*, 150–162, doi:10.1016/j.jmarsys.2008.08.007.
- Li, C., A. Valle-Levinson, K.-C. Wong, and K. M. M. Lwiza (1998), Separating baroclinic flow from tidally induced flow in estuaries, *J. Geophys. Res.*, *103*, 10,405–10,417, doi:10.1029/98JC00582.
- Li, C., A. Valle-Levinson, L. P. Atkinson, and T. C. Royer (2000), Inference of tidal elevation in shallow water using a vessel-towed acoustic Doppler current profiler, *J. Geophys. Res.*, *105*, 26,225–26,236, doi:10.1029/1999JC000191.
- Li, C., J. O. Blanton, and C. Chen (2004), Mapping of tide and tidal flows using vessel towed ADCP, *J. Geophys. Res.*, *109*, C04002, doi:10.1029/2003JC001992.
- Li, C., C. Chen, D. Guadagnoli, and I. Y. Georgiou (2008), Geometry-induced residual eddies in estuaries with curved channels: Observations and modeling studies, *J. Geophys. Res.*, *113*, C01005, doi:10.1029/2006JC004031.
- Li, C., E. Swenson, E. Weeks, and J. White (2009), Asymmetric tidal straining across an inlet: Lateral inversion and variability over a tidal cycle, *Estuarine Coastal Shelf Sci.*, *85*, 651–660, doi:10.1016/j.ecss.2009.09.015.
- Li, C., H. Roberts, G. Stone, E. Weeks, and Y. Luo (2011), Wind surge and salt-water intrusion in Atchafalaya Bay under onshore winds prior to cold front passage, *Hydrobiologia*, *658*, 27–39, doi:10.1007/s10750-010-0467-5.
- Li, M., and L. Zhong (2009), Flood-ebb and spring-neap variations of mixing, stratification and circulation in Chesapeake Bay, *Cont. Shelf Res.*, *29*, 4–14, doi:10.1016/j.csr.2007.06.012.
- Linden, P. F., and J. E. Simpson (1988), Modulated mixing and frontogenesis in shallow seas and estuaries, *Cont. Shelf Res.*, *8*, 1107–1127, doi:10.1016/0278-4343(88)90015-5.
- Makarewicz, J. C., T. W. Lewis, I. Bosch, M. R. Noll, N. Herendeen, R. D. Simon, J. Zollweg, and A. Vodacek (2009), The impact of agricultural best management practices on downstream systems: Soil loss and nutrient chemistry and flux to Conesus Lake, New York, USA, *J. Great Lakes Res.*, *35*, 23–36, doi:10.1016/j.jglr.2008.10.006.
- Marmor, H. A. (1948), The currents in Barataria Bay, report, 30 pp., Tex. A&M Res. Found., College Station, Tex.
- Murray, S. P. (1998), An observational study of the Mississippi-Atchafalaya coastal plume: Final report, *OCS Study MMS Rep. 98-0040*, 513 pp., Gulf of Mex. Outer Cont. Shelf Reg., Miner. Manage. Serv., U. S. Dep. of the Inter., New Orleans, La.
- Nahlik, A. M., and W. J. Mitsch (2008), The effect of river pulsing on sedimentation and nutrients in created Riparian wetlands, *J. Environ. Qual.*, *37*, 1634–1643, doi:10.2134/jeq2007.0116.
- Nunes, R. A., and G. W. Lennon (1987), Episodic stratification and gravity currents in a marine environment of modulated turbulence, *J. Geophys. Res.*, *92*, 5465–5480, doi:10.1029/JC092iC05p05465.
- Nunes Vaz, R. A., G. W. Lennon, and J. R. de Silva Samarasinghe (1989), The negative role of turbulence in estuarine mass transport, *Estuarine Coastal Shelf Sci.*, *28*, 361–377, doi:10.1016/0272-7714(89)90085-1.
- Park, D. (2002), Hydrodynamics and freshwater diversion within Barataria Basin, Ph.D. dissertation, 112 pp., La. State Univ., Baton Rouge.
- Rabalais, N. N., and R. E. Turner (Eds.) (2001), *Coastal Hypoxia: Consequences for Living Resources and Ecosystems*, *Coastal Estuarine Stud. Ser.*, vol. 58, AGU, Washington, D. C.
- Rabalais, N. N., R. E. Turner, B. K. Sen Gupta, D. F. Boesch, P. Chapman, and M. C. Murrell (2007a), Hypoxia in the northern Gulf of Mexico: Does the science support the plan to reduce, mitigate and control hypoxia?, *Estuaries Coasts*, *30*, 753–772.
- Rabalais, N. N., R. E. Turner, B. K. Sen Gupta, E. Platon, and M. L. Parsons (2007b), Sediments tell the history of eutrophication and hypoxia in the northern Gulf of Mexico, *Ecol. Appl.*, *17*, suppl., S129–S143, doi:10.1890/06-0644.1.
- Ralston, D. K., and M. T. Stacey (2007), Tidal and meteorological forcing of sediment transport in tributary mudflat channels, *Cont. Shelf Res.*, *27*, 1510–1527, doi:10.1016/j.csr.2007.01.010.
- RD Instruments (1996), *Acoustic Doppler Current Profiler Principles of Operation—A Practical Primer*, 57 pp., Poway, Calif.
- Rego, J., and C. Li (2009a), On the receding of storm surge along Louisiana's low-lying coast, *J. Coastal Res.*, *56*, 1045–1049.
- Rego, J., and C. Li (2009b), Numerical experiments and an overlooked parameter in storm surge forecasting: The forward speed of a hurricane, *Geophys. Res. Lett.*, *36*, L07609, doi:10.1029/2008GL036953.
- Rego, J., and C. Li (2010a), Nonlinear terms in storm surge predictions: Effect of tide and shelf geometry with case study from Hurricane Rita, *J. Geophys. Res.*, *115*, C06020, doi:10.1029/2009JC005285.
- Rego, J., and C. Li (2010b), Storm surge propagation in Galveston Bay during Hurricane Ike, *J. Mar. Syst.*, *82*, 265–279, doi:10.1016/j.jmarsys.2010.06.001.
- Rippeth, T. P., N. R. Fisher, and J. H. Simpson (2001), The cycle of turbulent dissipation in the presence of tidal straining, *J. Phys. Oceanogr.*, *31*, 2458–2471, doi:10.1175/1520-0485(2001)031<2458:TCOTDI>2.0.CO;2.
- Roberts, H. H., R. D. Adams, and R. H. W. Cunningham (1980), Evolution of sand-dominant subaerial phase, Atchafalaya Delta, Louisiana, *Am. Assoc. Pet. Geol. Bull.*, *64*, 264–279.
- Roberts, H. H., O. K. Huh, S. A. Hsu, L. J. Rouse Jr., and D. A. Rickman (1989), Winter storm impacts on the Chenier Plain Coast of southwestern Louisiana, *Trans. Gulf Coast Assoc. Geol. Soc.*, *39*, 515–522.
- Roberts, H. H., N. Walker, R. Cunningham, G. P. Kemp, and S. Majersky (1997), Evolution of sedimentary architecture and surface morphology: Atchafalaya and Wax Lake Deltas, Louisiana (1973–1994), *Trans. Gulf Coast Assoc. Geol. Soc.*, *47*, 477–484.
- Rouse, L. J., and J. M. Coleman (1976), Circulation observations in the Louisiana Bight using LANDSAT Imagery, *Remote Sens. Environ.*, *5*, 55–66, doi:10.1016/0034-4257(76)90035-3.
- Simpson, J. H., J. Brown, J. Matthews, and G. Allen (1990), Tidal straining, density currents, and stirring in the control of estuarine stratification, *Estuaries*, *13*, 125–132, doi:10.2307/1351581.
- Simpson, J. H., E. Williams, L. H. Brasseur, and J. M. Brubaker (2005), The impact of tidal straining on the cycle of turbulence in a partially stratified estuary, *Cont. Shelf Res.*, *25*, 51–64, doi:10.1016/j.csr.2004.08.003.
- Snedden, G. A. (2006), River, tidal and wind interactions in a deltaic estuarine system, Ph.D. dissertation, 116 pp., La. State Univ., Baton Rouge.
- Stacey, M. T., and D. K. Ralston (2005), The scaling and structure of the estuarine bottom boundary layer, *J. Phys. Oceanogr.*, *35*, 55–71, doi:10.1175/JPO-2672.1.
- Swenson, E. M., and C. M. Swarzenski (1995), Water levels and salinity in the Barataria-Terrebonne Estuarine system, in *Status and Trends of Hydrologic Modification, Reduction in Sediment Availability, and Habitat Loss/Modification in the Barataria and Terrebonne Estuarine System*, *Barataria-Terrebonne Natl. Estuarine Program Publ. Ser.*, vol. 20, edited by D. J. Reed, pp. 130–215, Barataria-Terrebonne Natl. Estuary Program, Thibodaux, La.
- Uthicke, S., and K. Nobes (2008), Benthic foraminifera as ecological indicators for water quality on the Great Barrier Reef, *Estuarine Coastal Shelf Sci.*, *78*, 763–773, doi:10.1016/j.ecss.2008.02.014.
- Walker, N. D., and A. B. Hammack (2000), Impacts of winter storms on circulation and sediment transport: Atchafalaya-Vermillion Bay region, Louisiana, U.S.A., *J. Coastal Res.*, *16*, 996–1010.
- Walker, N., W. J. Wiseman Jr., L. J. Rouse Jr., and A. Babin (2005), Effects of river discharge, wind stress, and slope eddies on circulation and the satellite-observed structure of the Mississippi River plume, *J. Coastal Res.*, *21*, 1228–1244, doi:10.2112/04-0347.1.
- Wang, L., and D. Justic (2009), A modeling study of the physical processes affecting the development of seasonal hypoxia over the inner Louisiana-Texas shelf: Circulation and stratification, *Cont. Shelf Res.*, *29*, 1464–1476, doi:10.1016/j.csr.2009.03.014.
- White, J. R., R. D. DeLaune, C. Y. Li, and S. Bentley (2009a), Distribution of methyl and total mercury in Louisiana and Georgia shelf sediments, *Anal. Lett.*, *42*, 1219–1231, doi:10.1080/00032710902901947.
- White, J. R., R. W. Fulweiler, C. Y. Li, S. Bargu, N. D. Walker, R. R. Twilley, and S. E. Green (2009b), Mississippi River flood of 2008: Observations of a large freshwater diversion on physical, chemical and biological characteristics of a shallow estuarine lake, *Environ. Sci. Technol.*, *43*, 5599–5604.

Wong, K.-C. (1994), On the nature of transverse variability in a coastal plain estuary, *J. Geophys. Res.*, 99, 14,209–14,222, doi:10.1029/94JC00861.

C. Chen and H. Lin, Department of Fisheries Oceanography, Intercampus Graduate School for Marine Science and Technology, University of Massachusetts, New Bedford, MA 02744, USA.

S. Bargu, K. Galvan, C. Li, E. Weeks, and J. R. White, Department of Oceanography and Coastal Sciences, Louisiana State University, Baton Rouge, LA 70803, USA. (cli@lsu.edu)